Frequency-narrowed diode array bar

Earl Babcock, Bien Chann, Ian A. Nelson, and Thad G. Walker

We describe a method to frequency narrow multielement high-power diode bars. Using a commercial 60-W, 49-element, 1-cm-long diode array bar at 795 nm running at 45 W, we narrow the linewidth from 1000 to 64 GHz with only a loss of 33% in output power. The resulting laser light is well suited for spin-exchange optical pumping of noble gas nuclei.

OCIS codes: 140.3600, 020.0020.

1. Introduction

Spin-exchange optical pumping (SEOP) places unique and demanding requirements on its laser source, requiring high power within the absorption profile of an alkali vapor, typically Rb. SEOP of ^{3}He and ^{129}Xe has many applications in both applied science and fundamental research.[1,2] These applications include a contrast agent for pulmonary, vascular, and brain magnetic resonance imaging,[3–5] precision measurements,[6–10] quantum computation,[11] and neutron spin filters,[12] the first and last being of particular interest to our laboratory. Both uses require production of large volumes of polarized noble gas with the highest polarization possible and hence a capable optical pumping source.

In SEOP, resonance circularly polarized pump light is absorbed by alkali atoms, usually Rb, contained in a sealed glass cell. The transition of interest is $^2S_{1/2} \rightarrow {}^2P_{1/2}$ at 795 nm. For most practical applications the hyperfine levels are not resolved because of the pressure broadening by the noble gas.[13] Hence, all the hyperfine levels are pumped equally. The alkali atoms become spin polarized, then their polarization is transferred to the noble gas nuclei through collisions.

E. Babcock (edbabcock@wisc.edu), B. Chann, and T. G. Walker are with the Department of Physics, University of Wisconsin-Madison, Madison, Wisconsin 53706. B. Chann is also with the Quantum Electronics Group L-146, MIT Lincoln Laboratory, Lexington, Massachusetts 02420. I. A. Nelson is with the Department of Human Oncology, University of Wisconsin Medical School, Madison, Wisconsin 53792.

Received 4 October 2004; accepted 3 December 2004.
0003-6935/05/153098-07$15.00/0

The rate of polarization of the noble gas is given by

$$[X]\frac{dP_{He}}{dt} = \frac{\Delta\Phi\eta}{V}, \tag{1}$$

where $\Delta\Phi$ is the absorbed photon flux, η is the Rb–noble-gas spin-exchange efficiency, V is the cell volume, and $[X]$ is the noble gas density. Here the ideal absorbed photon flux is given by

$$\Delta\Phi_{ideal} = \frac{\Gamma R_P}{R_P + \Gamma}[A]V, \tag{2}$$

where Γ is the alkali relaxation rate, R_P is the pumping rate, and $[A]$ is the alkali density. From Eqs. (1) and (2) it is apparent that, to maximize $\Delta\Phi$ and dP_{He}/dt, one desires $R_P \gg \Gamma$. The pumping rate is given by

$$R_P = \int_0^\infty I(\nu)\sigma(\nu)d\nu \simeq \frac{P\pi r_e f c}{A\Delta\nu}, \tag{3}$$

where $I(\nu)$ is the intensity of the pumping laser per unit frequency, $\sigma(\nu) = \pi r_e f c g(\nu)$ is the Rb absorption cross section where $g(\nu)$ is a normalized Lorenzian, A is the cross-sectional area of the cell being pumped, and $P/\Delta\nu$ is the power per unit frequency or spectral power that is the figure of merit used to attain high polarization in SEOP.

The most common laser used in SEOP is the diode array bar (DAB) because it can provide power up to hundreds of watts relatively easily and inexpensively compared with the other options at 795 nm, namely, dye or Ti:sapphire lasers.[14] However, the linewidth of a typical DAB is ≈1000 GHz (2 nm), which is much larger than the absorption linewidth of the Rb atoms

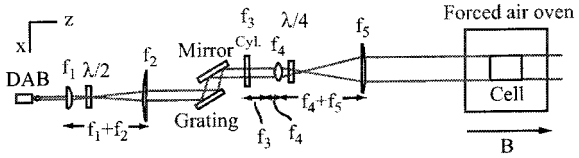

Fig. 1. Diagram of a frequency-narrowed DAB in an optical pumping apparatus.

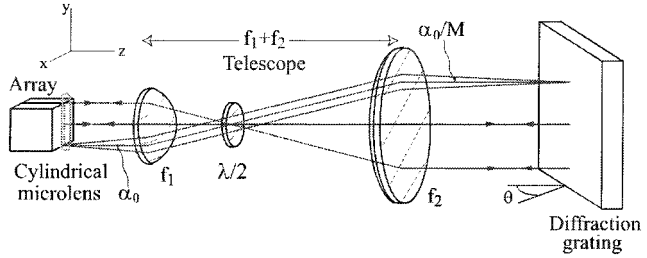

Fig. 2. Diagram showing the basic components and selected rays of the external-cavity DAB cavity.

that is 20 GHz/bar.[13] Conventionally, high ^{3}He or ^{4}He pressures (3–10 bars) are used to broaden the absorption linewidth, but even at 10 bars much of the light cannot be absorbed. In addition, some applications such as neutron spin filters prefer low-pressure cells ≈1 bar, which further limits the efficiency of our using a standard DAB source.

Attempts have been made to increase the efficiency of diode arrays for optical pumping. Diode arrays of one to two emitters (2–4 W) have been narrowed with external cavities and used for SEOP, showing improved performance.[15,16] Furthermore, the author of Ref. 17 describes a method to narrow the linewidth of a 40-W DAB by 50% using an etalon to provide feedback, and the authors of Ref. 18 use an external cavity to achieve single-mode (120-MHz) operation from a 2-W single-emitter diode array. For our method, first described in Ref. 19 and now extended for use at the Rb optical pumping wavelength of 795 nm, we use an external cavity to narrow the linewidth of a DAB by as much as a factor of 15.

As a direct comparison, a frequency-narrowed DAB running at 30 W with a linewidth of 65 GHz produces a pumping rate of 1.6×10^6/s for a typical 5-cm-diameter, 0.8-bar pressure cell whereas an unnarrowed DAB running at 60 W and 1000 GHz has a pumping rate of only 2×10^5/s. To look at it in another way, the frequency-narrowed DAB under the above conditions can produce the same pumping rate as 400 W of standard commercially available DAB power. However, even if one chose to do this it would be impractical for experimental use because of difficulties created by cell heating at high laser powers.[20] A diagram showing a typical optical pumping apparatus with a frequency-narrowed diode array bar is shown in Fig. 1.

Our results from extensive comparisons between our frequency-narrowed DAB and standard DABs are given in Ref. 21 showing the clear experimental advantages of this laser source. In this paper we give an in-depth description of the theory and operation of the frequency-narrowed DAB and detail the alignment procedures to build one.

2. External-Cavity Diode Array Bar

A common way to narrow and tune low-power single-mode diode lasers is to use an external cavity in the Littrow configuration.[22] In this cavity the laser acts as a near point source with diffraction-limited divergence in both directions so it can be collimated by a single fast aspherical lens. The collimated output is then reflected off a grating. The first order from the diffraction grating is used as a feedback to tune the frequency and reduce the linewidth. The zeroth order is taken as the output.

Use of an external cavity for a DAB is more difficult. Each DAB consists of a large number of broad-area lasers or emitters (typically 10–50) arranged in a length of 1 cm. The dimension of each emitter is typically 1 μm by 100 μm with a separation between emitters of 200–500 μm. Light emitted perpendicular to the array (fast axis) has a typical diffraction-limited divergence of 40 deg, and light emitted parallel to the array (slow axis) has a divergence of 10 deg and is multispatial mode. The asymmetric divergence of the individual emitters requires use of extra collimation optics. Next, since each of these many emitters has its own spatial mode they cannot be collimated together with one lens, and thus the Littrow condition would not be satisfied for each emitter simultaneously. Last, most DABs are not straight; there is a small curvature of the emitter alignment (a smile) that further complicates the imaging of the DAB. This smile is usually ≈2–10 μm and can greatly limit the ability to narrow an array in many cases. A picture of the smile of several DABs is shown in Fig. 6. Consequently the simple cavity described above does not work for a DAB, but we have shown that a slightly more complex version is effective.[20]

The cavity that we developed is shown in Fig. 2. Most DABs are currently available with fast axis collimation that consists of a cylindrical microlens attached directly to the front of the DAB. This cylindrical microlens forms the first critical element of the external cavity. Next an afocal telescope is used to image each emitter onto a Littrow-mounted grating with a constant diffraction angle θ for the ideal no-smile case as is shown in Fig. 2. Typical magnification of the telescope is ≈4–5. The frequency-selected first-order diffraction from each emitter is then reimaged back onto itself, while the zeroth order forms the output. If the DAB does not have an attached, prealigned cylindrical microlens, we describe in Subsections 3.A and 3.B how to mount and position one by hand.

The general form for the feedback condition in a Littrow cavity for light striking the grating with direction $\hat{z}\cos\alpha\cos\phi + \hat{y}\sin\alpha + \sin\phi$ with respect to the optical axis is

$$\lambda = 2d\,\sin(\theta - \phi)\cos\alpha, \tag{4}$$

or

$$\delta\lambda/\lambda_0 \approx -\alpha^2/2 - \phi \cot \theta, \quad (5)$$

where θ is the angle between the optical axis and the grating normal and satisfies the condition $\lambda_0 = 2d \sin \theta$, α is the divergence of the light along the slow axis, and ϕ is the angular spread due to the smile, both of which contribute to broadening of the narrowed laser spectrum. $\delta\lambda = \lambda - \lambda_0$ and the angles α and ϕ are assumed to be small.

The term depending on α represents broadening due to the multimode angular distribution of a single emitter along the slow axis. The ϕ term vanishes in the absence of smile. From Fig. 2, the telescope reduces the angular spread from the laser α_0 by a factor inversely proportional to the magnification of the telescope or $\alpha = \alpha_0/M$, where M is magnification of the telescope. Thus, from approximation (5) this reduces the α contribution to the laser linewidth by the square of the magnification.

The afocal nature of the telescope causes the angular spread of rays at the grating from off-axis elements to be symmetrically centered around zero, providing improved performance over finite focal-length imaging lens systems that were also attempted. The telescope reduces angular spread due to the smile to $\phi = x/Mf_c$, where x is the deviation of the laser output from the ideal straight, vertical output caused by the smile of the laser and f_c is the focal length of the microlens. The smile contribution to the linewidth is then

$$\frac{d\lambda}{\lambda} = \frac{x \cot \theta}{Mf_c}. \quad (6)$$

Consequently it is easy to see how a large magnification telescope along with a large diffraction angle θ work to minimize the broadening effects caused by smile.

Although we have tested many DABs, we report here narrowing a 60-W, 49-emitter array with fast axis collimation from Nuvonyx Inc. The array was selected by the manufacturer to have a smile of ≈ 1 μm and a center wavelength of 798 nm. The cavity used consists of a telescope with plano–convex lenses in which the convex surfaces are mounted inward as shown in Fig. 1 providing a magnification $M = 4$, a 40 mm $\times$ 40 mm 2400-lines/mm holographic grating, and a $\lambda/2$ plate. Exploiting the different S and P polarization efficiencies of the holographic grating allows the feedback to be adjusted by rotating the $\lambda/2$ plate. The output of the zeroth-order beam was set at $\approx$70% of the free-running power by rotating the $\lambda/2$ plate, and the free-running wavelength was set to 795 nm by adjusting the temperature of the laser cooling water to $\approx$15 °C. The linewidth was measured with a homemade parallel-plate scanning Fabry–Perot spectrometer. Table 1 shows the performance of our cavity with the Nuvonyx array for various output powers.

Table 1. Laser Performance

Current (A)	Unnarrowed Power (W)	Narrowed Power (W)	Efficiency (%)	FWHM (GHz)
50	45	30	67	64
37	30	21	70	61
28	20	14.5	72.5	51

Next we set the narrowed output to a moderate power of 16 W and adjusted the wavelength by merely changing the angle of the diffraction grating. Figure 3 shows the tuning range and spectral power of the external-cavity DAB demonstrating a tuning range of over 7 nm at the half-power points; at the highest output powers this range decreases slightly to $\approx$4–5 nm. Here the unnarrowed spectrum was obtained with an Ocean Optics Inc. S2000 spectrometer. Also it is important to note that the tuning range can be extended by adjusting the temperature. These DABs have a temperature coefficient of 2.4 nm/10 °C, consequently the center of the pattern in Fig. 3 can be shifted within the limits of the cooling system and the laser specifications.

To more fully quantify the full line shape of the laser, we greatly increased the free spectral range (FSR) of our parallel-plate Fabry–Perot spectrometer by simply moving the mirrors closer together. To accurately determine the shape of the unnarrowed output as well as provide a good estimate of the proportion of power in the narrowed peak under normal operating conditions, the narrowed peak was tuned approximately 0.5 nm away from the center of the free-running laser output allowing the two contributions to be resolved. The FSR of nearly 2 nm required for this measurement caused the instrumental function of our Fabry–Perot to became significant compared to the linewidth of the narrowed portion of the spectrum; therefore the linewidth of the narrowed portion had to be measured with the Fabry–Perot set to a lower FSR. Figure 4 shows a composite of the unnarrowed portion of the spectrum taken with a FSR of 2 nm with the narrowed peak removed and the narrowed portion taken with a FSR of 0.3 nm. The respective widths for the fits are

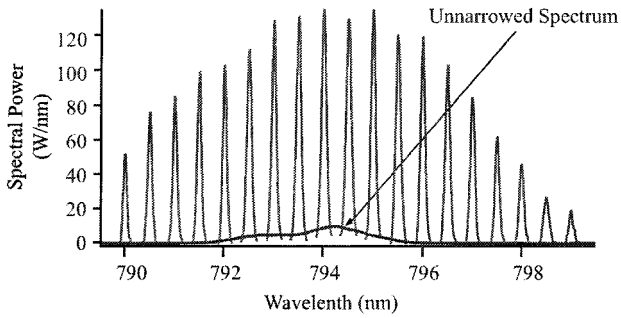

Fig. 3. Tuning range and spectral power density of the external-cavity DAB. The spectral density of the narrowed array is approximately ten times greater than the free-running power density.

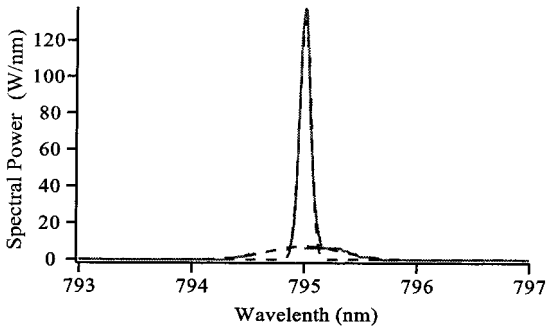

Fig. 4. Spectral profile of the frequency-narrowed DAB. The dashed curves are Gaussian fits. Approximately 75% of the power is in the narrow peak.

0.9 nm or 430 GHz for the broad background and 0.14 nm or 60 GHz for the narrowed peak with approximately 75% of the power in the narrowed peak.

We also successfully narrowed a variety of other DABs including 19-emitter, 40-W, 795-nm lasers from Coherent Inc., which did not have fast axis collimation, and several 17- to 20-W, 46-emitter, 795–801-nm lasers from CEO with and without fast axis collimation. Using a typical laser from Coherent Inc. with a smile of $\approx 2\ \mu m$, we obtained 14 W of power out of ≈22-W free running. In this case the measured spectral linewidth was 125 GHz at 795 nm whereas for a particular CEO laser with a 1-μm smile running at 12.2 W out of 18-W free running the linewidth was only 47 GHz. The increased linewidth was largely due to the contribution from the smile; from Eq. (6) the additional contribution to the spectral width just from the smile is ≈40 GHz/μm. Second, from the data with the Nuvonyx laser in Table 1 there is also a slight broadening associated with higher output powers.

We recently reported extensive comparisons between SEOP with a spectrally narrowed Coherent array and standard free-running DAB's; the complete details of these tests are provided in Ref. 21. With the Coherent array running narrowed with a 14-W output at a 125-GHz linewidth, the measured Rb polarization was >99% at a temperature as high as 180 °C in a cylindrical cell with a diameter of 4.7 cm and a length of 4.9 cm. Using 42 W of unnarrowed DAB power (22 W from an unnarrowed Coherent DAB and 20 W from two Spectra-Physics DABs), the Rb polarization under the same conditions was only 77%. In this cell, which has a ^{3}He wall relaxation time of 240 h, the observed ^{3}He polarization was as high as 73% compared with 59% with the unnarrowed arrays. The highest ^{3}He polarization we have produced to date using one of our external-cavity DABs was 81% in a 3-bar, 22.5-cm^3 cell. To our knowledge, this is the highest ^{3}He polarization ever obtained with a DAB. Further results from our ongoing research in hybrid SEOP have shown that, under certain conditions, unnarrowed DABs are unable to produce alkali polarizations as high as those obtained with our frequency-narrowed DAB regardless of the amount of power.[23]

3. Detailed Alignment Procedure

The alignment procedures for building an external-cavity DAB are listed in detail in Subsections 3.A–3.D. Here it is assumed that the DAB is already mounted and operational with the appropriate power supply and adequate cooling source. In Subsections 3.A and 3.B we explain the alignment of the microlens to the array bar. If the DAB has fast axis collimation from the manufacturer, Subsections 3.A and 3.B can be skipped altogether.

A. Mount Microlens

To obtain the needed degrees of freedom to align the cylindrical microlens it must be mounted in a mount that allows at least a three-axis rotational adjustment. We use a Newport GM-1R wave-plate holder mounted on a two-axis (x, z) translation stage. To mount the microlens in the wave-plate holder we mill a 2-cm-diameter hole in a solid insert, then mill a 1.5-mm-diameter groove, semicircular in cross section, across the insert. The microcylindrical lens is then attached into the groove with glue and the assembly is put into the wave-plate holder. To ensure that the lens can be placed close enough to the DAB, on the order of 1 mm, the microlens must protrude from the surface of the mount and the machined insert.

B. Align Microlens

The microlens and translational stage assembly is positioned directly in front of the DAB, ensuring that the center of the microlens and the center of the DAB are at the same height. Then the vertical axis of the DAB is approximately aligned with the vertical axis of the microlens. The DAB is then turned on just above its threshold current, and the output is observed on a screen ≈1 m away. Then the microlens is adjusted carefully though an iterative process until the lens is aligned exactly with the DAB and the fast axis is collimated. At this point the beam size is a few millimeters across, and the microlens will be close to the emitting face of the DAB. Figure 5 shows a picture of the DAB mounted on the diode mount with the microlens aligned in front of it.

C. Align Telescope

The first telescope lens is placed ($f = 62$ mm) at $z \simeq f_1$, making sure that the lens is aligned in the vertical and horizontal direction with the DAB such that the light from the center of the DAB passes through the center of the lens. The beam is projected onto a large screen or wall several meters from the DAB, and the lens is moved back and forth until the individual emitters of the DAB are imaged in the vertical direction forming individual rectangular spots on the screen. Then the $\lambda/2$ plate is placed a few centimeters from the first lens somewhere near its focal plane so that the entire beam can pass through cleanly. Now the second telescope lens ($f = 250$ mm) is placed at $z \simeq 2f_1 + f_2$, making sure that the vertical and horizontal position of the beam is

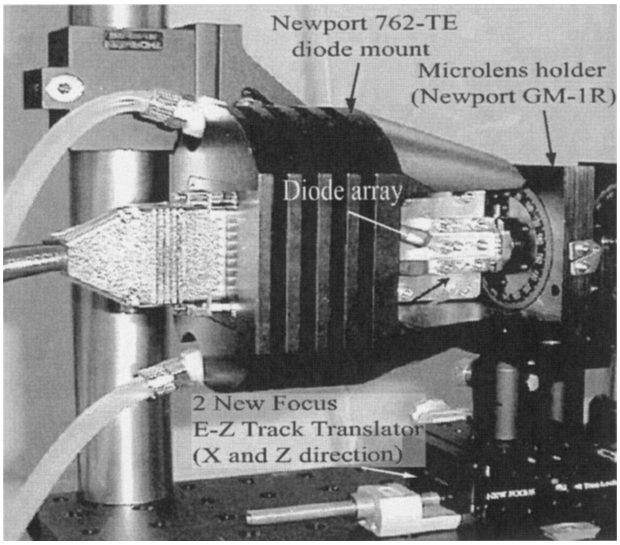

Fig. 5. Picture of diode array on the mount with the microlens aligned.

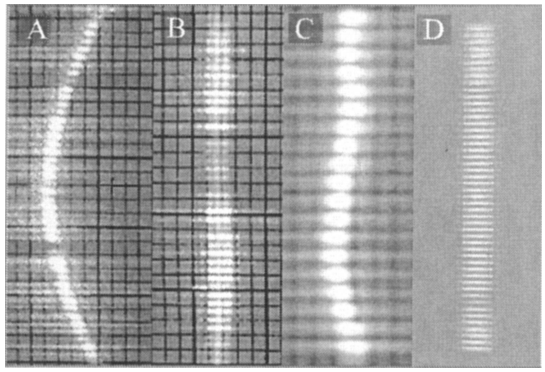

Fig. 6. Picture showing the images of four different DABs. Note the smile or curvature of the laser. A, picture of a 7-μm smile, 46-element CEO laser; B, a 1-μm smile, 46-element CEO laser; C, a 19-element Coherent laser with a 2-μm smile; D, a 49-element Nuvonyx laser with <1-μm smile.

aligned with the DAB. Now this lens is adjusted until the horizontal axis is collimated. Figure 1 shows this arrangement. Note that the lenses shown are plano–convex, the preferred choice for minimum aberrations, although in practice we find that a biconvex f_1 performs adequately. If the screen is sufficiently far from the array, this will be when the horizontal direction is the narrowest. At this point the beam should be a narrow vertical stripe on the screen.

D. Mount and Position Grating

The grating we chose was a 40 mm × 40 mm, 2400-lines/ mm holographic grating. We used this grating to accommodate the magnified output of the DAB, to obtain a large diffraction angle at $\lambda = 794$ nm, and to provide the desired feedback efficiency. This grating is mounted on a three-rotational-axis wave-plate holder to obtain the required degrees of freedom for optimal alignment and tuning. The grating is therefore mounted on a GM-1R wave-plate holder in the same way as the microlens, but this time the grating is simply glued to the front of an unmodified insert. At $z \simeq 2f_1 + 2f_2$ there should be a 4× magnified image of the array with the individual emitters forming sharp rectangular spots in a vertical row as in Fig. 6. The grating is positioned in this image plane, making sure that the grooves of the grating are along the vertical direction. Last, the power output is measured and the $\lambda/2$ plate is rotated until maximum power output is obtained (i.e., minimum feedback). This is to obtain the greatest sensitivity to the feedback alignment as further adjustments are made as well as to ensure that the DAB is not damaged with excessive feedback.

E. Adjust Feedback

Once all the lenses and grating are in place, a spectrometer is used to observe the frequency of the array output in real time; we use an Ocean Optics S2000. Care must be taken to make sure that the spectrometer samples all the diode bar elements equally since each emitter essentially acts as a separate laser. A good method is to focus the output beam onto a small spot on a holographic diffuser. The spectrometer is then placed behind the diffuser to sample the light. The angle and tilt of the grating is now adjusted to allow the first-order diffraction light to propagate back to the laser collinear with the original output beam and thus provide the feedback. A narrow peak above a broad background should show up on the spectrometer. The wavelength of this peak can be changed by adjusting the grating angle.

Most likely the external-cavity diode array is not working optimally yet and needs further adjustments. From our experience, the most sensitive adjustments are the microlens and the grating. The goal is to maximize the proportion of power in the tuning peak. Slight adjustments are made to the tilt and rotation of the grating while observing the output on the spectrometer. Once that is maximized, further improvement can sometimes be made with the microlens by adjusting the z position. Extreme caution should be taken with this adjustment because the microlens is very close (< 1 mm) to the DAB. Once all these adjustments are maximized, the feedback is adjusted with the $\lambda/2$ plate until the desired spectrum is obtained. Usually, the feedback required for optimal operation is ≈30% of the free-running power output. Finally the laser current is adjusted to obtain the desired power output.

To maintain long lifetimes of our DABs, we do not let the intercavity power exceed the rating of the DAB. The intercavity power is simply the power of the laser before the diffraction grating plus the power being feed back, which is equal to the power before the grating minus the power after the grating. Running in this regime we obtained DAB lifetimes of over a year running continuously. Consequently we do not believe that the external cavity shortens the normal 10,000-h DAB lifespan by an appreciable amount. We note that one may be able to run a frequency-

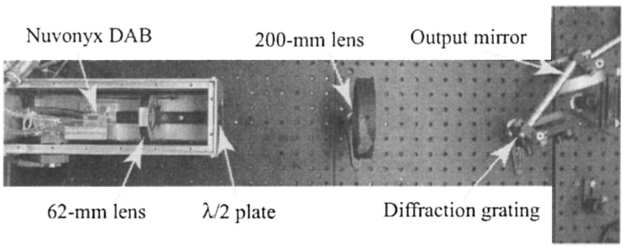

Fig. 7. External-cavity DAB.

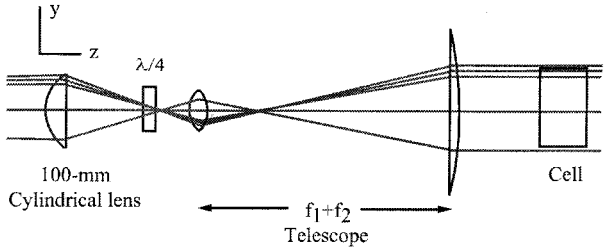

Fig. 8. Ray-tracing optical setup for the external diode array laser coupling to the cell; the z axis is scaled by 50% relative to the y axis. The grating, not shown, is at $z = 0$. In this example, $f_1 = 25$ mm and $f_2 = 250$ mm. The cell is typically overfilled to ensure uniform Rb polarization. Again, note that in practice f_2 is biconvex.

narrowed DAB at higher output powers, perhaps approaching the free-running power specification. However, we have not attempted any tests of DAB lifetimes under such conditions. Figure 7 shows a picture of the external-cavity DAB.

The highly spatially asymmetric output of the laser is efficiently coupled to a cell by the optical setup as shown in Fig. 8. We have shown that one should use collimated light in optical pumping.[24] One can normally achieve this by using a cylindrical lens to first focus the elongated laser output to a 4–5-mm square. Then a telescope of arbitrary magnification (10× in this case) is used to produce the desired collimated beam size. Shown in Fig. 8 is a setup used to pump a typical cell with a diameter of 47 mm. Again we note that the ideal choices for the lenses are shown; however, in practice we use a biconvex f_2 for this telescope that performs adequately. Depending on the experimental conditions, a variation of this scheme can be implemented.

To achieve a fixed direction of the output of the cavity as the laser is tuned, and thus a constant input into the cell coupling optics, we place a mirror as shown in Fig. 1. This mirror is mounted such that it remains parallel to the grating as the Littrow diffraction angle is changed, thus fixing the output in a constant direction. Figure 7 shows this mirror that is attached to a standard kinematic mount and is mounted to the top of the grating mount by simple posts.

4. Conclusions

We have demonstrated a versatile method for frequency narrowing and tuning various types of diode array bars. The resulting output is highly suited to the demands of efficient spin-exchange optical pumping. With the current technology it is possible to achieve powers in excess of 30 W at a linewidth of 65 GHz or less with only a 33% loss in output power. We anticipate that if this same technique were applied to an antireflection-coated DAB, one could obtain even higher output efficiencies and a wider tuning spectrum as is currently achieved in external cavities with low-power, single-mode antireflection-coated diodes that are now commonly commercially available.

This research was supported by the National Science Foundation and the U.S. Department of Energy. Tom Gentile, Dennis Rich, and Alan Thompson of the National Institute of Standards and Technology provided the ^{3}He cells. We benefited from many helpful discussions with Tom Gentile.

References

1. T. G. Walker and W. Happer, "Spin-exchange optical pumping of noble-gas nuclei," Rev. Mod. Phys. **69,** 629–642 (1997).
2. S. Appelt, A. Ben-Amar Baranga, C. J. Erickson, M. V. Romalis, A. R. Young, and W. Happer, "Theory of spin-exchange optical pumping of ^{3}He and ^{129}Xe," Phys. Rev. A **58,** 1412–1439 (1998).
3. M. S. Albert, G. D. Cates, B. Driehuys, W. Happer, C. S. Springer, Jr., B. Saam, and A. Wishnia, "Biological magnetic resonance imaging using laser-polarized ^{129}Xe," Nature (London) **370,** 199–201 (1994).
4. D. A. Lipson, D. A. Roberts, J. Hansen-Flaschen, T. R. Gentile, G. Jones, A. Thompson, I. E. Dimitrov, H. I. Palevsky, J. S. Leigh, M. Schnall, and R. R. Rizi, "Pulmonary ventilation and perfusion scanning using hyperpolarized helium-3 MRI and arterial spin tagging in healthy normal subjects and in pulmonary embolism and orthotopic lung transplant patients," Magn. Reson. Med. **47,** 1073–1076 (2002).
5. H. E. Moller, X. J. Chen, B. Saam, K. D. Hagspiel, G. A. Johnson, T. A. Altes, E. E. de Lange, and H.-U. Kauczor, "MRI of the lungs using hyperpolarized noble gases," Magn. Res. Med. **47,** 1029–1051 (2002).
6. D. Bear, R. E. Stoner, R. L. Walsworth, V. A. Kostelecky, and C. D. Lane, "Limit on Lorentz and CPT violation of the neutron using a two-species noble-gas maser," Phys. Rev. Lett. **85,** 5038–5041 (2000).
7. N. R. Newbury, A. S. Barton, P. Bogorad, G. D. Cates, M. Gatzke, B. Saam, L. Han, R. Holmes, P. A. Souder, and J. Xu, "Laser polarized muonic helium," Phys. Rev. Lett. **67,** 3219–3222 (1991).
8. Y. Masuda, J. D. Bowman, R. D. Carlini, T. Case, T. E. Chupp, K. P. Coulter, S. J. Freedman, T. R. Gentile, M. Gericke, G. L. Greene, F. W. Hersmann, T. Ino, S. Ishimoto, G. L. Jones, M. B. Leuschner, G. S. Mitchell, K. Morimoto, S. Muto, H. Nann, S. A. Page, S. I. Penttila, W. D. Ramsay, E. I. Sharapov, T. B. Smith, W. M. Snow, S. W. Wilburn, and Y. W. Yuan, "Parity-violating gamma-ray asymmetry in the neutron-proton capture," Nucl. Phys. A **721,** 485c–488c (2003).
9. M. V. Romalis and M. P. Ledbetter, "Transverse spin relaxation in liquid ^{129}Xe in the presence of large dipolar fields," Phys. Rev. Lett. **87,** 067601/1-4 (2001).
10. W. Xu, D. Dutta, F. Xiong, B. Anderson, L. Auberbach, T. Averett, W. Bertozzi, T. Black, J. Calarco, L. Cardman, G. D. Cates, Z. W. Chai, J. P. Chen, S. Choi, E. Chudakov, S. Churchwell, G. S. Corrado, C. Crawford, D. Dale, A. Deur, P. Djawotho, B. W. Filippone, J. M. Finn, H. Gao, R. Gilman, A. V.

Glamazdin, C. Glashausser, W. Glckle, J. Golak, J. Gomez, V. G. Gorbenko, J.-O. Hansen, F. W. Hersman, D. W. Higinbotham, R. Holmes, C. R. Howell, E. Hughes, B. Humensky, S. Incerti, C. W. de Jager, J. S. Jensen, X. Jiang, C. E. Jones, M. Jones, R. Kahl, H. Kamada, A. Kievsky, I. Kominis, W. Korsch, K. Kramer, G. Kumbartzki, M. Kuss, E. Lakuriqi, M. Liang, N. Liyanage, J. LeRose, S. Malov, D. J. Margaziotis, J. W. Martin, K. McCormick, R. D. McKeown, K. McIlhany, Z.-E. Meziani, R. Michaels, G. W. Miller, E. Pace, T. Pavlin, G. G. Petratos, R. I. Pomatsalyuk, D. Pripstein, D. Prout, R. D. Ransome, Y. Roblin, M. Rvachev, A. Saha, G. Salm, M. Schnee, T. Shin, K. Slifer, P. A. Souder, S. Strauch, R. Suleiman, M. Sutter, B. Tipton, L. Todor, M. Viviani, B. Vlahovic, J. Watson, C. F. Williamson, H. Witala, B. Wojtsekhowski, J. Yeh, and P. Zolnierczuk, "Transverse asymmetry A_T from the quasielastic He $- - >(e - - >, e')$ process and the neutron magnetic form factor," Phys. Rev. Lett. **85,** 2900–2904 (2000).

11. A. S. Verhulst, O. Liivak, M. H. Sherwood, H. M. Vieth, and I. L. Chuang, "Non-thermal nuclear magnetic resonance quantum computing using hyperpolarized xenon," Appl. Phys. Lett. **79,** 2480–2482 (2001).
12. W. C. Chen, C. Bailey, J. A. Borchers, R. F. C. Farrow, T. R. Gentile, D. Hussey, C. F. Majkrzak, K. V. O'Donovan, N. Remmes, W. M. Snow, and A. K. Thompson, "Polarized ^{3}He analyzers for neutron reflectometry," Physica B. **335,** 196–200 (2003).
13. M. V. Romalis, E. Miron, and G. D. Cates, "Pressure broadening of Rb D_1 and D_2 lines by ^{3}He, ^{4}He, N_2, and Xe: line cores and near wings," Phys. Rev. A **56,** 4569–4578 (1997).
14. B. Driehuys, G. D. Cates, E. Miron, K. Sauer, D. K. Walter, and W. Happer, "High-volume production of laser-polarized ^{129}Xe," Appl. Phys. Lett. **69,** 1668–1670 (1996).
15. I. A. Nelson, B. Chann, and T. G. Walker, "Spin-exchange optical pumping using a frequency-narrowed high power diode laser," Appl. Phys. Lett. **76,** 1356–1358 (2000).
16. J. N. Zerger, M. J. Lim, K. P. Coulter, and T. E. Chupp, "Polarization of ^{129}Xe with high power external-cavity laser diode arrays," Appl. Phys. Lett. **76,** 1798–1800 (2000).
17. M. V. Romalis, "Narrowing of high power diode laser arrays using reflection feedback from an etalon," Appl. Phys. Lett. **77,** 1080–1081 (2000).
18. S. B. Bayram and T. E. Chupp, "Operation of a single mode external-cavity laser diode array near 780 nm," Rev. Sci. Instrum. **73,** 4169–4171 (2002).
19. B. Chann, I. Nelson, and T. G. Walker, "Frequency-narrowed external-cavity diode-laser-array bar," Opt. Lett. **25,** 1352–1354 (2000).
20. D. K. Walter, W. M. Griffith, and W. Happer, "Energy transport in high-density spin-exchange optical pumping cells," Phys. Rev. Lett. **86,** 3264–3267 (2001).
21. B. Chann, E. Babcock, L. W. Anderson, T. G. Walker, W. C. Chenn, T. B. Smith, A. K. Thompson, and T. R. Gentile, "Production of highly polarized ^{3}He using spectrally narrowed diode laser array bars," J. Appl. Phys. **94,** 6908–6914 (2003).
22. C. Wieman and L. Hollberg, "Using diode lasers for atomic physics," Rev. Sci. Instrum. **62,** 1–20 (1991).
23. E. Babcock, I. Nelson, S. Kadlecek, B. Driehuys, L. W. Anderson, F. W. Hersman, and T. G. Walker, "Hybrid spin-exchange optical pumping of ^{3}He," Phys. Rev. Lett. **91,** 123003/1-4 (2003).
24. B. Chann, E. Babcock, L. W. Anderson, and T. G. Walker, "Skew light propagation in optically thick optical pumping cells," Phys. Rev. A **66,** 033406/1-3 (2002).